

1 Towards a Pixel TPC part I: construction and test of a  
2 32-chip GridPix detector

3 M. van Beuzekom<sup>a</sup>, Y. Bilevych<sup>b</sup>, K. Desch<sup>b</sup>, S. van Doesburg<sup>a</sup>,  
4 H. van der Graaf<sup>a</sup>, F. Hartjes<sup>a</sup>, J. Kaminski<sup>b</sup>, P.M. Kluit<sup>a</sup>,  
5 N. van der Kolk<sup>a</sup>, C. Ligtenberg<sup>a</sup>, G. Raven<sup>a</sup>, J. Timmermans<sup>a</sup>

6 <sup>a</sup>*Nikhef, Science Park 105, 1098 XG Amsterdam, The Netherlands*

7 <sup>b</sup>*Physikalisches Institut, University of Bonn, Nussallee 12, 53115 Bonn,*  
8 *Germany*

---

9 **Abstract**

10 A Time Projection Chamber (TPC) module with 32 GridPix chips was con-  
11 structed and the performance was measured using data taken in a testbeam  
12 at DESY in 2021. The GridPix chips each consist of a Timepix3 ASIC  
13 (TPX3) with an integrated amplification grid and have a high efficiency of  
14 about 85% to detect single ionisation electrons. In the testbeam setup, the  
15 module was placed in between two sets of Mimosas26 silicon detector planes  
16 that provided external high-precision tracking and the whole detector setup  
17 was slid into the PCMag magnet at DESY. The TPC could be operated  
18 reliably and used a 93.6/5.0/1.4 gas mixture (by volume) of Ar/iC<sub>4</sub>H<sub>10</sub>/CO<sub>2</sub>  
19 with a small amount of oxygen and water vapour. The analysed data were  
20 taken at electron beam momenta of 5 and 6 GeV/c and at magnetic fields of  
21 0 and 1 T.

22 The result for the transverse diffusion coefficient  $D_T$  is  $(287.2 \pm 0.5)$   
23  $\mu\text{m}/\sqrt{\text{cm}}$  at  $B = 0$  T and  $D_T$   $(120.3 \pm 0.5)$   $\mu\text{m}/\sqrt{\text{cm}}$  at  $B = 1$  T. The  
24 longitudinal diffusion coefficient  $D_L$  is measured to be  $(251 \pm 14)$   $\mu\text{m}/\sqrt{\text{cm}}$

---

\*Corresponding author, Telephone: +31 20 592 2000  
*Preprint submitted to Nuclear Instruments and Methods A*  
Email address: s01@nikhef.nl (P.M. Kluit)

25 at  $B = 0$  T and  $(224 \pm 14) \mu\text{m}/\sqrt{\text{cm}}$  at  $B = 1$  T. Results for the tracking  
26 systematical uncertainties in  $xy$  (pixel plane) were measured to be  $13 \mu\text{m}$   
27 with and without magnetic field. The tracking systematical uncertainties in  
28  $z$  (drift direction) were smaller than  $15 \mu\text{m}$  ( $B = 0$  T) and  $20 \mu\text{m}$  ( $B = 1$   
29 T).

30 *Keywords:*

31 Micromegas, gaseous pixel detector, micro-pattern gaseous detector,  
32 Timepix, GridPix, pixel time projection chamber

---

## 33 1. Introduction

34 Earlier publications on a single chip [1] and four chip (quad) GridPix de-  
35 tectors [2] showed the potential of the GridPix technology and the large range  
36 of applications for these devices [3]. In particular, it was demonstrated that  
37 single ionisation electrons can be detected with high efficiency and accuracy,  
38 allowing excellent 3D track position measurements and particle identification  
39 based on the number of electrons and clusters.

40 As a next step towards a Pixel Time Projection Chamber for a future  
41 collider experiment [4, 5], a module consisting of 32 GridPix chips based on  
42 the TPX3 chip was constructed.

43 A GridPix detector consists of a CMOS pixel TPX3 chip [6] with inte-  
44 grated amplification grid added by photo-lithographic - Micro-electromechanical  
45 Systems (MEMS) - post-processing techniques. The TPX3 chip can be op-  
46 erated with a low threshold of  $515 e^-$ , and has a low equivalent noise charge  
47 of about  $70 e^-$ . The GridPix single chip and quad detectors have a very  
48 fine granularity of  $55 \times 55 \mu\text{m}^2$  with  $256 \times 256$  pixels per chip. The device has

49 a high efficiency of about 85% - discussed in this paper - to detect single  
50 ionisation electrons.

51 Based on the experience gained with these detectors a 32-GridPix detector  
52 module - consisting of 8 quad detectors - was built. A drift box defining the  
53 electric field and gas envelope was constructed. A read out system for up  
54 to 128 chips with 4 multiplexers read out by one Speedy Pixel Detector  
55 Readout (SPIDR) board [7, 8] was designed. After a series of tests using  
56 the laser setup [9] and cosmics in the laboratory at Nikhef, the detector was  
57 taken to DESY for a two week testbeam campaign.

58 At DESY, the 32-chip detector was placed in between two sets of Mi-  
59 mosa26 silicon detector planes and mounted on a movable stage. The whole  
60 detector setup was slid into the centre of the PCMAG magnet at DESY.  
61 A beam trigger was provided by scintillator counters. The data reported  
62 here were taken at different stage positions and electron beam momenta of  
63 5 and 6 GeV/c and at magnetic fields of 0 and 1 T. The performance of the  
64 32-GridPix detector module was measured using these data sets.

65 In this paper, part I of the results will be presented with the main focus on  
66 the detector spatial resolution and tracking performance. A second follow-up  
67 paper will discuss the  $dE/dx$  (or  $dN/dx$ ) and other results.

## 68 **2. The 32-GridPix detector module**

69 A 32-GridPix detector module was built using the quad detector module  
70 [2] as a basic building block. The quad module consists of four GridPix chips  
71 and is optimised for a high fraction of sensitive area of 68.9%. The external  
72 dimensions are 39.60 mm  $\times$  28.38 mm. The four chips which are mounted

73 on a cooled base plate (COCA), are connected with wire bonds to a common  
74 central 6 mm wide PCB. A 10 mm wide guard electrode is placed over the  
75 wire bonds 1.1 mm above the aluminium grids, in order to prevent field  
76 distortions of the electric drift field. The guard electrode is the main inactive  
77 area, and its dimensions are set by the space required for the wire bonds.  
78 On the back side of the quad module, the PCB is connected to a low voltage  
79 regulator. The aluminium grids of the GridPix detectors are connected by  
80 80  $\mu\text{m}$  insulated copper wires to a high voltage (HV) filtering board. The  
81 quad module consumes about 8 W of power of which 2 W is used in the LV  
82 regulator.

83 Eight quad modules were embedded in a box, resulting in a GridPix  
84 detector module with a total of 32 chips. A schematic 3-dimensional drawing  
85 of the detector is shown in Figure 1. A schematic drawing of the quad  
86 detectors in the module is shown in Figure 2, where also the beam direction  
87 is indicated.

88 The internal dimensions of the box are 79 mm along the  $x$ -axis, 192 mm  
89 along the  $y$ -axis, and 53 mm along the  $z$ -axis (drift direction), and it has a  
90 maximum drift length (distance between cathode and read out anode) of 40  
91 mm. The magnetic field is pointing in the  $z$  direction, orthogonal to the  $xy$   
92 plane. The drift field is shaped by a series of parallel CuBe field wires of 75  
93  $\mu\text{m}$  diameter with a wire pitch of 2 mm. Guard strips are located on all of  
94 the four sides of the active area. In addition, six guard wires - shown with  
95 dashed lines (one colored red) in Figure 2 - are suspended over the boundaries  
96 of the chips, to minimise distortions of the electric drift field. The wires are  
97 located at a distance of 1.15 mm from the grid planes, and their potential is

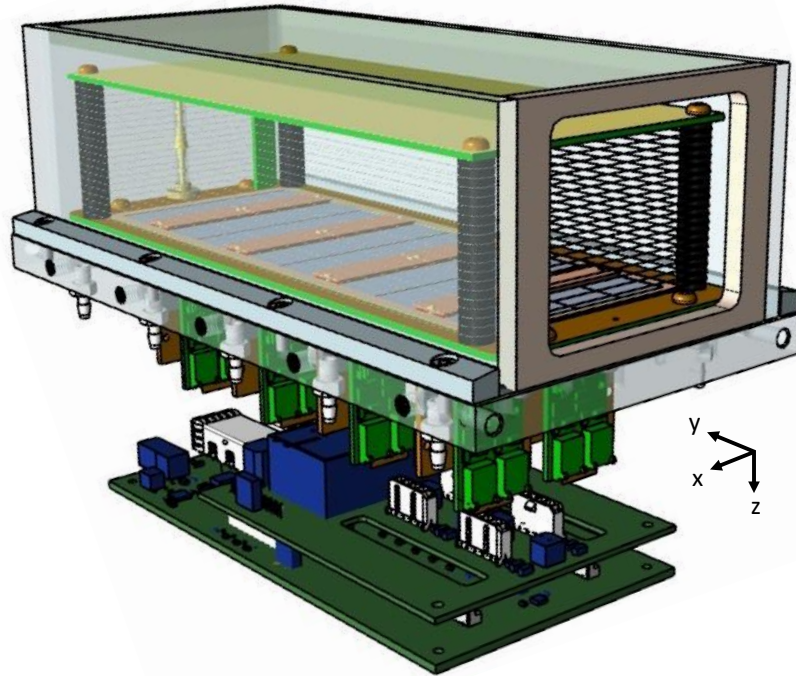


Figure 1: Schematic 3-dimensional rendering of the 32-GridPix module detector for illustration purposes.

98 set to the drift potential at this drift distance. The box has two  $50 \mu\text{m}$  thick  
 99 Kapton windows to allow the beam to pass with minimal multiple scattering.

100 The gas volume of 780 ml is continuously flushed at a rate of  $\sim 50 \text{ ml/min}$   
 101 (about 4 volumes/hour) with premixed T2K TPC gas. This gas is a mixture  
 102 consisting of 95% Ar, 3%  $\text{CF}_4$ , and 2%  $\text{iC}_4\text{H}_{10}$  suitable for large TPCs because  
 103 of the low transverse diffusion in a magnetic field and the high drift velocity.

104 The data acquisition system of the quad module was adopted to allow for  
 105 reading out multiple quad detectors. A multiplexer card was developed that  
 106 handles four quad detectors or 16 chips and combines the TPX3 data into  
 107 one data stream. For the 32-GridPix module two multiplexers are connected

108 to a SPIDR board that controls the chips and read out process. The read  
 109 out speed per chip is 160 Mbps and for the multiplexer 2.56 Gbps: this  
 110 corresponds to a maximum rate of 21 MHits/s. For each pixel the precise  
 111 Time of Arrival (ToA) using a 640 MHz TDC and the time over threshold  
 112 (ToT) are measured.

### 113 3. Experimental setup

114 In preparation of the two weeks DESY testbeam campaign, a support  
 115 frame was designed to move the 32-chip GridPix detector module in the  
 116 plane perpendicular to the beam by a remotely controlled stage such that  
 117 the whole detector volume could be probed. The module was mounted upside

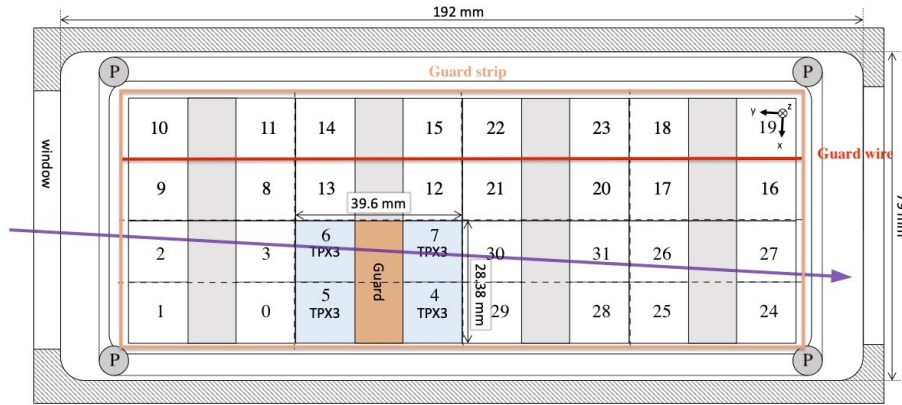


Figure 2: Schematic drawing of the 32-GridPix module detector with one example quad as viewed from the top of the quad detectors. The chips are numbered and the beam direction is shown in purple. A guard electrode of a quad detector is shown in orange. The four surrounding guard strips are shown -not to scale- in orange. Six guard wires - are shown with dashed lines (one colored red) and the pillars of the drift box are shown as circles with a P in the centre.

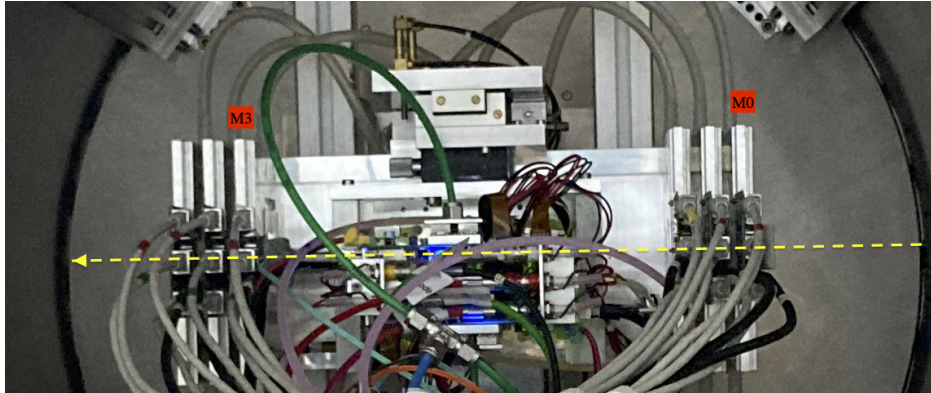


Figure 3: Photo of the detector setup - side view - at the centre of the PCMAG magnet (the circular contour). The Mimosa26 planes M0 and M3 are indicated in red as well as the beam direction (yellow).

118 down with respect to Figure 1 to allow access to the electronics from above.  
119 The support frame also held three Mimosa26 silicon detector planes [10] -  
120 with an active area of  $(21.2 \text{ mm} \times 10.6 \text{ mm})$  - placed in front of the detector  
121 and three Mimosa26 planes behind the detector. At DESY, the Mimosa26  
122 silicon detector planes were provided by the testbeam coordinators. The  
123 whole detector setup was slid towards the centre of the PCMAG magnet  
124 at the DESY II testbeam facility [10]. A beam trigger was provided by a  
125 double scintillator counter coincidence. The data were taken at different  
126 stage positions to cover the whole sensitive TPC volume. Runs with electron  
127 beam momenta of 5 and 6 GeV/c and at magnetic fields of 0 and 1 T were  
128 analysed.

129 A photograph of the detector setup in the PCMAG magnet is shown in  
130 Figure 3. The stage positions of the TPC module with respect to the beam  
131 and the Mimosa26 planes can be adjusted.

132 The experimental and environmental parameters such as temperature,  
 133 pressure, gas flow and oxygen content were measured and logged by a Win-  
 134 dows operated slow control system. The experimental parameters are sum-  
 135 marised in Table 1. The chips were cooled by circulating Glycol through  
 136 the cooling channels in the module carrier plate. The cooling blocks of the  
 137 multiplexers were further cooled by blowing pressurised air on them.

Table 1: Overview of the experimental parameters. The ranges indicate the variation over the data taking period

Number of analysed runs at $B=0$ (1) T	6 (8)
Run duration	10-90 minutes
Number of triggers per run	3-100 k
$E_{\text{drift}}$	280 V/cm
$V_{\text{grid}}$	340 V
Threshold	550 e <sup>-</sup>
Gas temperature	303.3-306.6 K
Pressure	1011 – 1023 mbar
Oxygen concentration	240 - 620 ppm
Water vapour concentration	2000 - 7000 ppm

138 The data was produced in four main data streams: one stream produced  
 139 by the Mimosas26 telescope, two data streams by the two Timepix multiplex-  
 140 ers and one trigger stream. The double scintillator coincidence provided a  
 141 trigger signal to the Trigger Logic Unit (TLU) [11] that sends a signal to the  
 142 telescope read out and the trigger SPIDR. The data acquisition systems of  
 143 the telescope and trigger SPIDR injected a time stamp into their respective



144 data streams. Hits from the Mimosas26 planes were collected with a sliding  
145 window of  $-115 \mu\text{s}$  to  $230 \mu\text{s}$  around the trigger time. The data acquisition  
146 of the multiplexer and the trigger SPIDR were synchronised at the start of  
147 the run. By comparing the time stamps in these streams, telescope tracks  
148 and TPC tracks could be matched. Unfortunately, the SPIDR trigger had  
149 - due to a cabling mistake at the output of the TLU - a common 25 ns flat  
150 time jitter.

151 After a short data taking period one of the chips (nr 11) developed a  
152 short circuit and the HV on the grid of the chip was disconnected. After the  
153 testbeam data taking period the module was repaired in the clean room in  
154 Bonn.

## 155 4. Analysis

### 156 4.1. Telescope track reconstruction procedure

157 The data of the telescope is decoded and analysed using the Corryvreckan  
158 software package [12]. The track model used for fitting was the General  
159 Broken Lines (GBL) software [14]. The code was extended and optimised to  
160 fit curved broken lines for the data with magnetic field. The telescope planes  
161 were iteratively aligned using the standard alignment software provided by  
162 the package. The single point Mimosas26 resolution is  $4 \mu\text{m}$  in  $x$  and  $6 \mu\text{m}$   
163 in  $z$  (drift direction) [10].

164 Telescope tracks were required to have hits in at least 5 out of the 6 planes  
165 and a total  $\chi^2$  of better than 25 per degree of freedom. The uncertainties on  
166 the telescope track prediction in the middle of the GridPix detector module  
167 are dominated by multiple scattering. The amount of multiple scattering

168 was estimated by comparing the predictions from the two telescope arms for  
 169 6 GeV/c tracks at  $B = 0$  T. The expected uncertainty in  $x$  and  $z$  is  $26 \mu\text{m}$   
 170 on average.

#### 171 4.2. TPC Track reconstruction procedure

172 GridPix hits are selected requiring a minimum time over threshold ToT  
 173 of  $0.15 \mu\text{s}$ . The drift time is defined as the measured time of arrival minus  
 174 the trigger time recorded in the trigger SPIDR data stream minus a fixed  $t_0$   
 175 (the drift time at zero drift). The drift time was corrected for time walk [2]  
 176 using the measured time over threshold (ToT in units of  $\mu\text{s}$ ) and the formula  
 177 (1):

$$\delta t = \frac{18.6(ns \mu s)}{\text{ToT} + 0.1577(\mu s)}. \quad (1)$$

178 Furthermore, small time shift corrections - with an odd-even and a  $16 \times$  pixels  
 179 structure - coming from the TPX3 clock distribution were extracted from the  
 180 data and applied.

181 The  $z$  drift coordinate was calculated as the product of the drift time  
 182 and the drift velocity. This implies that  $z_{\text{drift}} = -z$  as defined in Figure 1.  
 183 GridPix hits outside an acceptance window of 30 mm wide in  $x$  and 15 mm  
 184 wide in  $z$ , corresponding to the size of the entrance window, were not used  
 185 in the track finding and reconstruction. Based on a Hough transform an  
 186 estimate of the TPC track position and angles in the middle of the module  
 187 (at  $y = 1436$  pixels) were obtained. This estimate was used to collect the  
 188 hits around the TPC track and fit the track parameters.

189 The fit is performed separately in the  $xy$  and  $zy$  planes, using a linear  
 190 (for  $B = 0$  T data) or quadratic (for  $B = 1$  T data) track model in the  $xy$

Table 2: Table with track/event selection cuts

Track/Event Selection
$ x_{\text{TPC}} - x_{\text{telescope}}  < 0.3 \text{ mm}$
$ z_{\text{TPC}} - z_{\text{telescope}}  < 2 \text{ mm}$
$ dx/dy_{\text{TPC}} - dx/dy_{\text{telescope}}  < 4 \text{ mrad}$
$ dz/dy_{\text{TPC}} - dz/dy_{\text{telescope}}  < 2 \text{ mrad}$

191 plane (perpendicular to the magnetic field direction) and a linear model in  
 192 the  $zy$  plane. The fit minimizes the sum of squared distances between the  
 193 hits (associated to the pixel center in  $xy$ ) and the track, in both planes taking  
 194 into account the expected uncertainties  $\sigma_{xy}$  and  $\sigma_z$  (see Eqs. 2 and 3 ) The  
 195 fit was iterated three times to reject outlier hits at respectively 10, 5 and 2.5  
 196  $5 \sigma_{xy}$  or  $\sigma_z$ , respectively.

197 A TPC track was required to have at least 100 hits in each multiplexer.  
 198 At least 25% of the total number of hits should be on track and the  $\chi^2$  per  
 199 degree of freedom had to be less than 3 in  $xy$  and  $zy$ . All track parameters  
 200 were expressed at a plane in the middle of the TPC module.

201 The calibration and alignment of the detector was done using high quality  
 202 tracks for which the track selections are summarised in Table 2.

203 The drift velocity was calibrated per run by fitting a linear function to  
 204 the  $z$  (predicted from the telescope track at the measured TPC hit position)  
 205 versus the measured drift time in the TPC. For the  $B = 0$  T runs it varies  
 206 between 61.6 and 63.0  $\mu\text{m}/\text{ns}$ . For the  $B = 1$  T runs it is between 57.2 and  
 207 59.1  $\mu\text{m}/\text{ns}$ . The variation comes mainly from the changes in the relative  
 208 humidity of the gas volume due to small leaks.

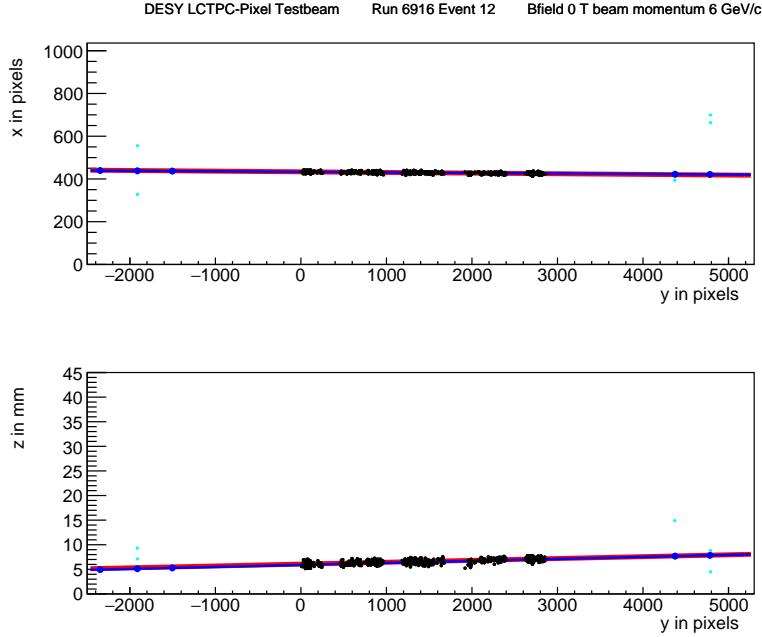


Figure 4: An event display for run 6916 without  $B$  field, with in total 1293 TPC hits (black dots) in the (top) precision plane  $(x, y)$  and (bottom) drift plane  $(z \text{ drift}, y)$ . The fitted TPC track (red line) with 1130 hits on track and the telescope track (blue line) with 5 Mimoso26 planes (blue hits) on track are shown. In green the off track Mimoso26 hits are shown.

209     The individual TPX3 chips were iteratively aligned fitting a shift in  $x$  ( $z$ )  
 210 and two slopes  $dx(z)/dx(y)$ . The alignment was done per run, because the  
 211 detector was moved in  $x$  and/or  $z$  for each run. The fitted slopes were also  
 212 corrected for small shifts and rotations (3D) in the nominal chip position.

213     An example event from run 6916 without  $B$  field with a TPC and a  
 214 telescope track is shown in Figure 4. The TPC is located between  $y = 0$  and  
 215 2872 pixels. Three Mimoso26 planes are located at  $y < -1000$  and three at  
 216  $y > 4000$  pixels.

## 217 5. Hit resolutions

218 The track residual in  $xy$  is defined as the closest distance - defined as the  
219 2D  $xy$  projection of the 3D distance - between the hit at the center of the  
220 pixel and the track. The residual in  $z$  is calculated at this point of closest  
221 approach. The single-electron hit resolutions in  $xy$  and  $z$  will be extracted  
222 from the track residuals. In order to study the single-electron resolution  
223 for the data with and without magnetic field, additional selections on the  
224 telescope and TPC tracks were applied. Due to the trigger time jitter of 25  
225 ns (corresponding to 1.5 mm drift), the prediction of the telescope track in  
226  $z$  must be used as the reference for  $z$ . Therefore the  $z$  hits of the TPC track  
227 were fitted to correct for the common time shift and the - biased -  $z$  residuals  
228 were calculated with respect to the fitted TPC track. In the  $xy$  plane the  
229 residuals of TPC hits with respect to the telescope track were used to extract  
230 the single-electron resolution in  $xy$ . For the resolution studies, runs at three  
231 different  $z$  stage positions of the TPC were selected where the beam gave  
232 hits in the central chips. The data of 14 central chips (9, 12, 21, 20, 17, 16,  
233 2, 3, 6, 7, 30, 31, 26 and 27) were used. Two chips (8 and 13) were left out  
234 because of the E field deformations caused by the short circuit in chip 11.

### 235 5.1. Hit resolutions in the pixel plane

236 The residual of the hits in the pixel plane ( $xy$ ) was measured as a function  
237 of the predicted drift position ( $z_{\text{drift}}$ ). The azimuthal angle  $\phi$  is defined as  
238  $\tan(\phi) = dx/dy$ . Tracks were selected that crossed the fiducial region defined  
239 by the central core of the beam. Hits were removed in a region of 20 pixels  
240 near the chip edges in  $x$ . The spread on the residual in  $xy$  for an ionisation

241 electron is given by:

$$\sigma_{xy}^2 = \sigma_{\text{track}}^2 + \frac{d_{\text{pixel}}^2(1 + \sin^2 2\phi)}{12} + D_T^2(z_{\text{drift}} - z_0), \quad (2)$$

242 where  $\sigma_{\text{track}}$  is the uncertainty from the track prediction,  $d_{\text{pixel}}$  is the pixel  
 243 pitch size,  $z_0$  is the position of the grid, and  $D_T$  is the transverse diffusion  
 244 coefficient. The last two terms correspond to the single-electron detector  
 245 resolution (squared). In the testbeam setup, the beam angle  $\phi$  is close to  
 246 zero and therefore the resolution at zero drift distance  $d_{\text{pixel}}/\sqrt{12}$  could be  
 247 fixed to  $15.9 \mu\text{m}$ . The track contribution  $\sigma_{\text{track}}$  was estimated to be  $30 \mu\text{m}$   
 248 for  $B = 0 \text{ T}$  and  $42 \mu\text{m}$  for  $B = 1 \text{ T}$  data. The uncertainty on the track  
 249 prediction was measured and is larger than the Mimosa plane resolution  
 250 because of multiple scattering in the sensors and in the entrance and exit  
 251 windows.

252 The expression (2) - leaving  $z_0$  and  $D_T$  as free parameters - is fitted  
 253 to the  $B = 0 \text{ T}$  data shown in Figure 5. The fit gives a transverse diffusion  
 254 coefficient  $D_T$  of  $(287.2 \pm 0.5) \mu\text{m}/\sqrt{\text{cm}}$ . The measured value is in agreement  
 255 with the value of  $287 \mu\text{m}/\sqrt{\text{cm}} \pm 4\%$  predicted by the gas simulation software  
 256 Magboltz 11.9 [15]. The values of the diffusion coefficients depend on the  
 257 humidity that was not precisely measured during the testbeam. The humidity  
 258 strongly affects the drift velocity. Therefore the drift velocity prediction from  
 259 Magboltz was used to determine the water content per run and predictions  
 260 for the diffusion coefficients could be obtained.

261 A fit to the  $B = 1 \text{ T}$  data, also shown in Figure 5, gives a transverse  
 262 diffusion coefficient  $D_T$  of  $(120.3 \pm 0.5) \mu\text{m}/\sqrt{\text{cm}}$ . The measured value is in  
 263 agreement with the value of  $119 \mu\text{m}/\sqrt{\text{cm}} \pm 2\%$  predicted by Magboltz.

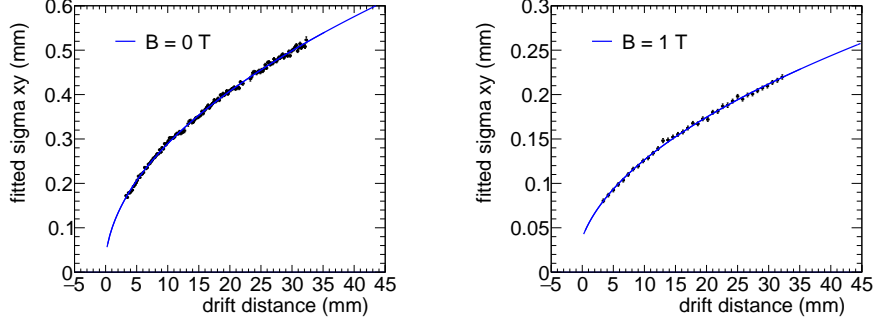


Figure 5: Measured spread on the residuals in the pixel plane (black points) for (left)  $B = 0$  T and (right)  $B = 1$  T, fitted with equation (2) (blue line).

## 264 5.2. Hit resolution in the drift plane

265 The spread on the residual in  $z$  of the ionisation electrons  $\sigma_z$  is given by:

$$\sigma_z^2 = \sigma_{\text{track}}^2 + \sigma_{z_0}^2 + D_L^2(z_{\text{drift}} - z_0), \quad (3)$$

266 where  $\sigma_{\text{track}}$  is the expected track uncertainty,  $\sigma_{z_0}$  the detector resolution at  
 267 zero drift distance and  $D_L$  the longitudinal diffusion constant. The last two  
 268 terms in the equation correspond to the single-electron detector resolution  
 269 (squared). Only tracks crossing the fiducial region - defined by the central  
 270 core of the beam - were accepted and hits with a ToT value above  $0.6 \mu\text{s}$   
 271 were selected. Because of the time jitter, the fitted TPC track is used for the  
 272 drift residuals. For  $z_{\text{drift}}$  the telescope prediction at the hit was used. The  
 273 expected uncertainty on TPC track prediction is propagated and amounts to  
 274  $50 \mu\text{m}$  at  $z = z_0$ . The systematic uncertainty on  $\sigma_{\text{track}}$  is estimated to be 25  
 275  $\mu\text{m}$ .

276 The expression (3) - leaving  $\sigma_{z_0}$  and  $D_L$  as free parameters - is fitted  
 277 to the  $B = 0$  T data shown in Figure 6. The value of  $z_0$  was fixed to the

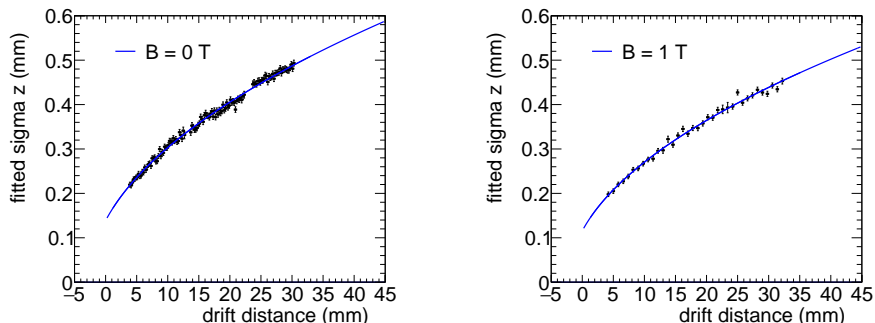


Figure 6: Measured spread on the residuals in the drift plane for hits with a ToT above  $0.60 \mu\text{s}$  for (left)  $B = 0 \text{ T}$  and (right)  $B = 1 \text{ T}$ . The data are fitted with the expression of equation (3).

278 result of the fit in the  $xy$  plane. The value of  $\sigma_{z0}$  was measured to be 129  
 279  $\mu\text{m}$ . The longitudinal diffusion coefficient  $D_L$  was determined to be  $(251$   
 280  $\pm 1$  (stat)  $\pm 14$  (sys))  $\mu\text{m}/\sqrt{\text{cm}}$ , which is higher than the expected value  
 281  $236 \pm 3 \mu\text{m}/\sqrt{\text{cm}}$  from a Magboltz calculation [15]. The quoted systematic  
 282 uncertainty on  $D_L$  is rather large and obtained from a fit using  $\sigma_{\text{track}} = 25$   
 283  $\mu\text{m}$ .

284 A fit to the  $B = 1 \text{ T}$  data shown in Figure 6 gives a longitudinal diffusion  
 285 coefficient  $D_L$  of  $(224 \pm 2$  (stat)  $\pm 14$  (sys))  $\mu\text{m}/\sqrt{\text{cm}}$ . The measured value  
 286 is lower than the value of  $(245 \pm 4) \mu\text{m}/\sqrt{\text{cm}}$  predicted by Magboltz. The  
 287 fitted value of  $\sigma_{z0}$  was  $114 \mu\text{m}$ .

### 288 5.3. Deformations in the pixel and drift plane

289 It is important to measure possible deformations in the pixel ( $xy$ ) and  
 290 drift ( $z$ ) plane to quantify the tracking precision. For the construction of  
 291 a large Pixel TPC, deformations in the pixel plane should be controlled to  
 292 better than typically  $20 \mu\text{m}$  because these affect the momentum resolution.



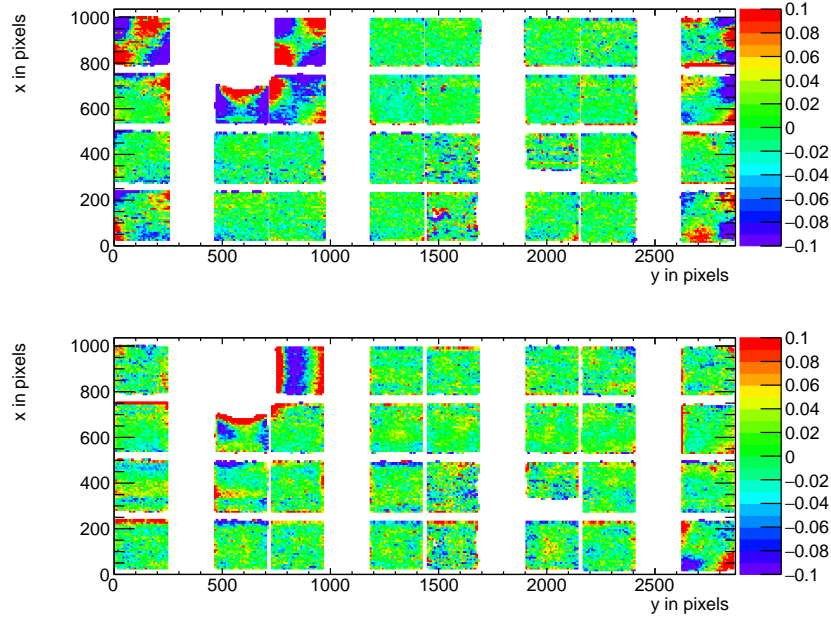


Figure 7: Mean residuals (color coded in mm) in the pixel (top) and drift (bottom) plane for  $B = 0$  T data at the expected hit position.

293 The mean residuals in the pixel and drift planes are shown in Figure 7 for  
 294 the  $B = 0$  T data set using a large set of runs to cover the whole module.  
 295 The residuals were calculated with respect to the telescope track prediction.  
 296 Because of limited statistics, groups of  $16 \times 16$  pixels were combined into one  
 297 bin. Bins with less than 100 hits are left out and residuals larger (smaller)  
 298 than  $+(-)100 \mu\text{m}$  are shown in red (blue).

299 A few critical areas can be observed in Figure 7: the region around chip 11  
 300 is affected (chips 14, 8 and 13), because the grid of chip 11 was disconnected.  
 301 Deformations are present at the four corners of the drift box (chips 1, 10,  
 302 19 and 24) and close to the right upper corner edge (chip 16) of the drift  
 303 box. These come from inhomogeneities in the drift field near the supporting

304 pillars, where the field wires are too close to the chip to provide a constant  
 305 electric field. It was concluded that for the deformation studies the hits of  
 306 these nine chips have to be removed. The track fit was redone leaving these  
 307 hits out of the fit, such that they could not bias and affect the results. Note  
 308 that a bias in the mean residual at the edge of the chips is expected to be  
 309 present for an ideal detector because of the finite coverage and the diffusion  
 310 in the drift process.

311 In order to reduce the statistical fluctuations and quantify the tracking  
 312 precision, the pixels were regrouped into larger bins respecting the module  
 313 geometry. After the regrouping procedure, a module plane with  $(4 \times 256) \times 256$   
 314 bins is obtained, as shown in Figure 8 <sup>1</sup>. The regrouping in  $(256, 4 \times 256)$   
 315 quantifies systematic uncertainties along the  $x$ -axis, while the regrouping in  
 316  $(4 \times 256, 256)$  bins quantifies systematic uncertainties along the  $y$ -axis. Bins  
 317 have a size of  $16 \times 16$  pixels and bins with less than 1000 entries are not  
 318 shown. Due to the presence of a so-called dike - that was created in the  
 319 TPX3 post-processing to protect the edges of the TPX3 chip - pixels at the  
 320 edge of the chip were covered and inefficient. Therefore, the region of 5  
 321 pixels in  $y$  near the edge of each chip was removed. For the drift coordinate  
 322 studies, a region of 10 pixels near the edge of each chip in  $x$  and  $y$  was  
 323 removed. The total number of measurements (bins) in  $xy$  is 895 and in  $z$   
 324 892. One can observe that in the module plane no clear systematic deviations

---

<sup>1</sup>The mathematical procedure is defined as follows. The original mean residual - before rebinning - is given by  $\text{residual}(i,j)$  where  $i$  runs horizontally and  $j$  vertically. The rebinned result for the residual  $(4 \times 256, 256)$  is equal to  $\text{residual}(i\%1024, j\%256)$ . The mean residual  $(256, 4 \times 256)$  - discussed later in the paper - is equal to  $\text{residual}(i\%256, j)$ .

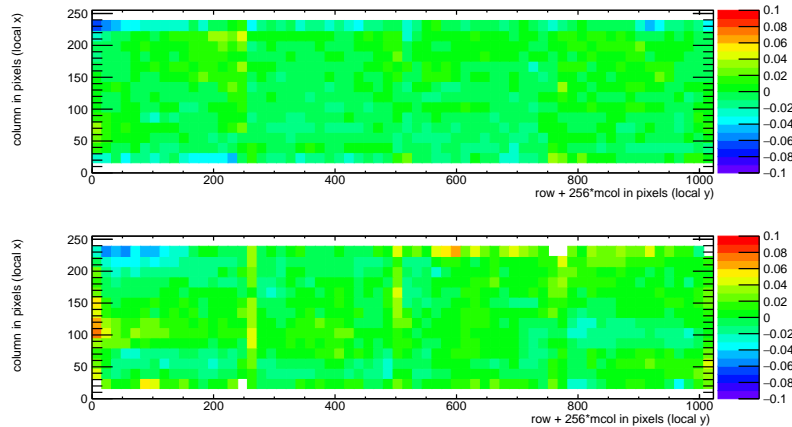


Figure 8: Mean residuals after regrouping (color coded in mm) in the pixel (top) and drift plane (bottom) for  $B = 0$  T data at the expected hit position.

325 are present and conclude that the guard wire voltages were on average well  
 326 tuned. Note that in the quad detector module we had no guard wires and  
 327 deformation corrections had to be applied [2]. The r.m.s. of the distribution  
 328 of the measured mean residual over the surface in the pixel plane is  $11 \mu\text{m}$   
 329 and in the drift plane  $15 \mu\text{m}$ . Similarly, regrouping the module in a plane  
 330 with  $256 \times (4 \times 256)$  pixel bins, yielded a r.m.s. in the pixel plane of  $13 \mu\text{m}$   
 331 and  $13 \mu\text{m}$  in the drift coordinate. The expected statistical error - obtained  
 332 by propagating the uncertainties on the residuals - in  $xy$  is  $4 \mu\text{m}$  and in  $z$   $5$   
 333  $\mu\text{m}$ .

334 In the  $B = 1$  T data set, the electrons will drift mainly along the magnetic  
 335 field lines. Deformations are in that case due to e.g. the non-alignment of the  
 336 electric and magnetic field, giving  $E \times B$  effects. Unfortunately, the statistics  
 337 of the telescope tracks that have a matched TPC track was insufficient and  
 338 did not cover the full TPC module plane. Therefore the larger statistics of

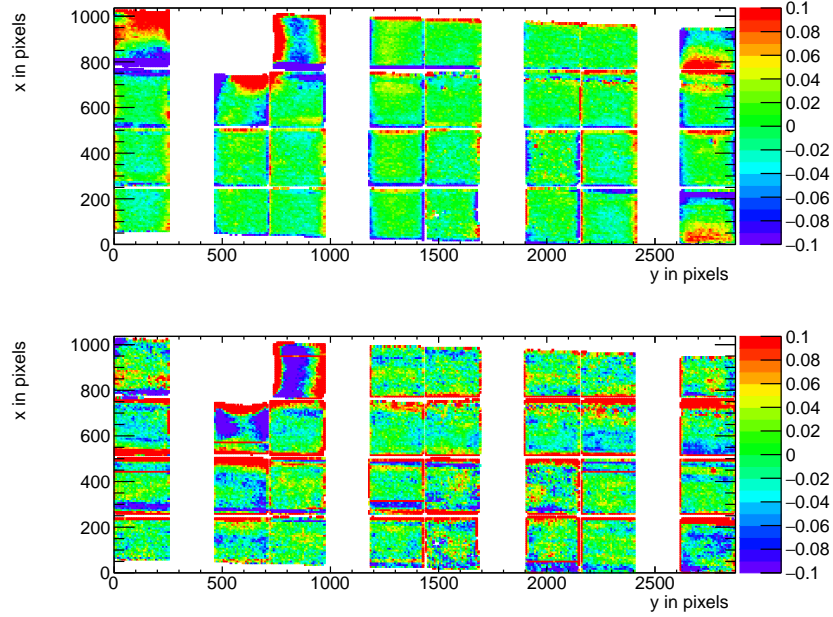


Figure 9: Mean residuals (color coded in mm) in the pixel (top) and drift plane (bottom) for  $B = 1$  T data at the expected hit position.

339 matched and unmatched TPC tracks was used. TPC tracks were required  
 340 to pass angular selection cuts ( $dx/dy$  between -40 and -20 mrad and  $dz/dy$   
 341 between 0 and 14 mrad) and a momentum cut ( $p > 2$  GeV/c and  $q < 0$ ).

342 The mean residuals in the pixel and drift planes are shown in Figure 9 for  
 343 the  $B = 1$  T data set using a large set of runs to cover the whole module. The  
 344 (biased) residuals were calculated with respect to the TPC track prediction.  
 345 Because of limited statistics, bins were grouped into  $16 \times 16$  pixels. Bins with  
 346 less than 100 hits are left out and residuals larger (smaller) than  $+(-)100 \mu\text{m}$   
 347 are shown in red (blue).

348 In Figure 9 the critical areas discussed above - around chip 11, the four  
 349 corner chips and chip 16 in the right upper corner edge - can be clearly

350 observed. For the deformation studies, the hits of these nine chips were  
351 removed. The TPC track fit was redone leaving these hits out of the fit,  
352 thus that they could not bias and affect the results. The TPC plane is well  
353 covered, although one can observe that due to the angle of the beam in the  
354  $xy$  plane the chips in the upper right and lower left corners are not fully  
355 covered.

356 In order to reduce the statistical fluctuations and quantify the tracking  
357 precision, the module was again regrouped in  $(4 \times 256) \times 256$  pixels as de-  
358 scribed above, as shown in Figure 10. Bins have a size of  $16 \times 16$  pixels and  
359 bins with less than 1000 entries are not shown. Similar to the no-field defor-  
360 mation studies, acceptance cuts had to be applied. The region of 16 pixels in  
361  $y$  near the edge of the chips was removed. For the drift coordinate studies,  
362 in addition a region of 10 pixels in  $x$  near the edge of the chip was removed.  
363 The total number of measurements (bins) in  $xy$  is 896 and in  $z$  896. One can  
364 observe that in the module plane no clear systematic deviations are present.  
365 The r.m.s. of the distribution of the measured mean residual over the surface  
366 in the pixel plane is  $13 \mu\text{m}$  and in the drift plane  $19 \mu\text{m}$ . Similarly, regroup-  
367 ing the module in  $256 \times (4 \times 256)$  pixel bins, yielded a r.m.s. in the pixel plane  
368 of  $11 \mu\text{m}$  and  $20 \mu\text{m}$  in the drift coordinate. The expected statistical error  
369 in  $xy$  is  $2 \mu\text{m}$  and in  $z$   $3 \mu\text{m}$ .

370 In summary, the deformation studies for the  $B = 0$  and 1 T data demon-  
371 strate that the systematical uncertainties in  $xy$  are  $13 \mu\text{m}$  with and without  
372 magnetic field. The systematical uncertainties in  $z$  were smaller than  $15 \mu\text{m}$   
373 ( $B = 0$  T) and  $20 \mu\text{m}$  ( $B = 1$  T).

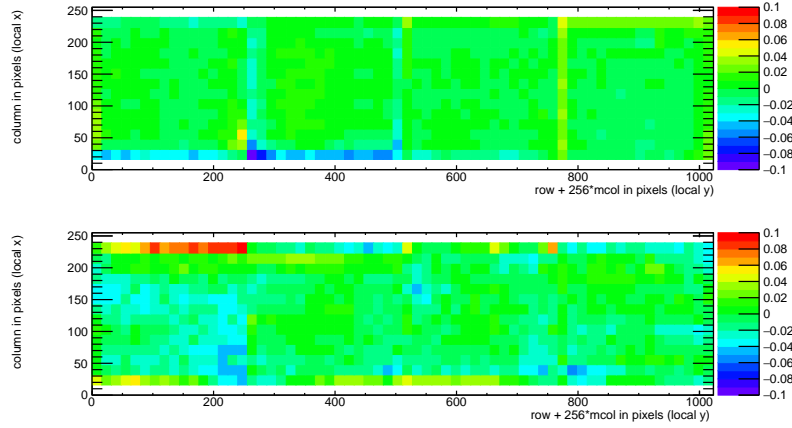


Figure 10: Mean residuals after regrouping (color coded in mm) in the pixel and drift plane for  $B = 1\text{T}$  data at the expected hit position.

374 *5.4. Tracking resolution*

375 A selected TPC track in the  $B = 0\text{ T}$  data has on average 1000 hits. The  
 376 tracking precision in the middle of the TPC (at  $y = 1436$  pixels) was derived  
 377 on a track-by-track basis, by propagating the pixel TPC hit uncertainties.  
 378 It was found to be on average  $9\ \mu\text{m}$  in the precision plane and  $13\ \mu\text{m}$  in  $z$ ,  
 379 with an rms width of  $2.4\ \mu\text{m}$  in  $xy$  and  $2.8\ \mu\text{m}$  in  $z$ . The angular resolution  
 380 in  $dx/dy$  was on average  $0.19\ \text{mrad}$  and for  $dz/dy$   $0.25\ \text{mrad}$ . It is clear that  
 381 the position resolution in the TPC in the precision and drift coordinates is  
 382 impressive for a track length of (only)  $158\ \text{mm}$ . The values are smaller than  
 383 the uncertainty on the track prediction from the silicon telescope of  $26\ \mu\text{m}$   
 384 in  $x$  and  $z$  on average that is dominated by multiple scattering.

## 385 6. Single electron efficiency

386 The distribution of the number of TPC track hits per chip - without  
387 requiring a matched telescope track - are shown in Figure 11 for the data  
388 without magnetic field and for the  $B = 1$  T data. For the  $B = 0$  T data, the  
389 central chips 2,6,7,9,16,17,26 and 27 were selected. For the  $B = 1$  T data,  
390 the same chips plus chips 12,13,20 and 21 were selected.

391 The mean number of hits is measured to be 124 and 89 in the  $B = 0$  T  
392 and 1 T data sets, respectively. The most probable values are respectively  
393 87 and 64. Note that the  $B = 0$  T data have a much larger Landau-like tail  
394 than the 1 T data. Also the fluctuations in the core of the distribution are  
395 larger. The mean time over threshold (ToT) is  $0.68 \mu\text{s}$  for the  $B = 0$  T and  
396  $0.86 \mu\text{s}$  at a  $B = 1$  T data. A typical ToT distribution can be found in Figure  
397 6 of [1] and Figure 5.5 of [4]. The time over threshold is related to the charge  
398 after avalanche multiplication. This means that the mean deposited charge  
399 per pixel is smaller for the 0 T data. The most probable value for the total  
400 deposited charge is similar for both data sets. A possible explanation for this  
401 behavior is that because of the reduced transverse diffusion in the  $B = 1$  T  
402 data, the possibility of two primary electrons ending up in a single grid hole  
403 is higher. The mean number of hits is in agreement with the prediction of  
404 106 electron-ion pairs for a 5 and 6 GeV/c electron at  $B = 0$  T for the T2K  
405 gas by [13], crossing 236 pixels or 12.98 mm and a detector running at 85%  
406 single-electron efficiency. The single-electron efficiency at this working point  
407 is in agreement with the efficiency vs mean time over threshold curve that  
408 was measured using a Fe source [4].

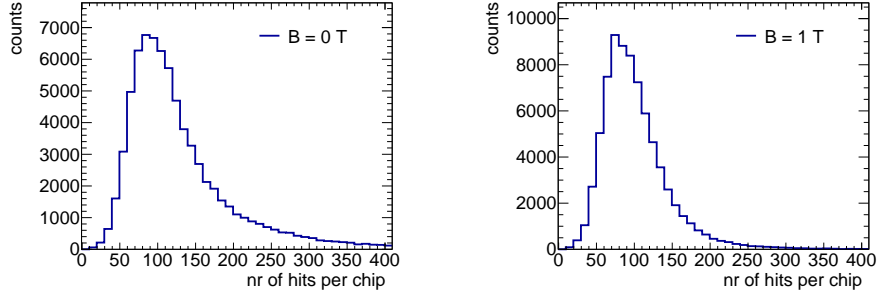


Figure 11: Distribution of the number of TPC track hits per chip for (left)  $B = 0$  T and (right)  $B = 1$  T data.

## 409 7. Conclusion and outlook

410 A TPC module with 32 GridPix chips was constructed and the perfor-  
 411 mance was measured using data taken in a testbeam at DESY in 2021. The  
 412 TPC could be operated reliably and used a 93.6/5.0/1.4 gas mixture (by vol-  
 413 ume) of Ar/ $i$ C<sub>4</sub>H<sub>10</sub>/CO<sub>2</sub> with a small amount of oxygen and water vapour.  
 414 The analysed data were taken at electron beam momenta of 5 and 6 GeV/ $c$   
 415 and at magnetic fields of 0 and 1 T.

416 The result for the transverse diffusion coefficient  $D_T$  is  $(287.2 \pm 0.5)$   
 417  $\mu\text{m}/\sqrt{\text{cm}}$  at  $B = 0$  T and  $D_T$  is  $(120.3 \pm 0.5) \mu\text{m}/\sqrt{\text{cm}}$  at  $B = 1$  T. The  
 418 longitudinal diffusion coefficient  $D_L$  is measured to be  $(251 \pm 14) \mu\text{m}/\sqrt{\text{cm}}$   
 419 at  $B = 0$  T and  $(224 \pm 14) \mu\text{m}/\sqrt{\text{cm}}$  at  $B = 1$  T. Results for the tracking  
 420 systematical uncertainties in  $xy$  were measured to be  $13 \mu\text{m}$  with and without  
 421 magnetic field. The tracking systematical uncertainties in  $z$  were smaller than  
 422  $15 \mu\text{m}$  ( $B = 0$  T) and  $20 \mu\text{m}$  ( $B = 1$  T).

423 The mean number of hits is in agreement with the predictions of [13] and  
 424 a detector running at 85% single-electron efficiency.



425 Not all data were analysed and users are welcome to study them using  
426 the data sets on available on the Grid <sup>2</sup>.

427 The GridPix detector will be further tested and developed in view of a  
428 TPC that will be installed in a heavy ion experiment at the EIC or other  
429 future colliders. A follow-up paper is in preparation on the measured  $dE/dx$   
430 or  $dN/dx$  resolution and other performance topics.

### 431 **Acknowledgements**

432 This research was funded by the Netherlands Organisation for Scientific  
433 Research NWO. The authors want to thank the support of the mechanical  
434 and electronics departments at Nikhef and the detector laboratory in Bonn.  
435 The measurements leading to these results have been performed at the Test  
436 Beam Facility at DESY Hamburg (Germany), a member of the Helmholtz  
437 Association (HGF).

### 438 **References**

- 439 [1] C. Ligtenberg, et al., Performance of a GridPix detector based  
440 on the Timepix3 chip, Nucl. Instrum. Meth. A 908 (2018) 18–23.  
441 arXiv:1808.04565, doi:10.1016/j.nima.2018.08.012.
- 442 [2] C. Ligtenberg, et al., Performance of the GridPix detector quad,  
443 Nucl. Instrum. Meth. A 956 (2020) 163331. arXiv:2001.01540,  
444 doi:10.1016/j.nima.2019.163331.

---

<sup>2</sup>For more information, please contact the corresponding author.

- 445 [3] J. Kaminski, Y. Bilevych, K. Desch, C. Krieger, M. Lupberger, GridPix  
446 detectors - introduction and applications, Nucl. Instrum. Meth. A845  
447 (2017) 233–235. doi:10.1016/j.nima.2016.05.134.
- 448 [4] C. Ligtenberg, A GridPix TPC read out for the ILD experiment at the  
449 future International Linear Collider, Ph.D. thesis, Free University of  
450 Amsterdam (2021). URL  
451 [https://www.nikhef.nl/pub/services/biblio/theses\\_pdf/thesis\\_C\\_Ligtenberg.pdf](https://www.nikhef.nl/pub/services/biblio/theses_pdf/thesis_C_Ligtenberg.pdf)
- 452 [5] M. Lupberger, Y. Bilevych, H. Blank, D. Danilov, K. Desch, A. Hamann,  
453 J. Kaminski, W. Ockenfels, J. Tomtschak, S. Zigann-Wack, To-  
454 ward the Pixel-TPC: Construction and Operation of a Large Area  
455 GridPix Detector, IEEE Trans. Nucl. Sci. 64 (5) (2017) 1159–1167.  
456 doi:10.1109/TNS.2017.2689244.
- 457 [6] T. Poikela, J. Plosila, T. Westerlund, M. Campbell, M. De Gaspari,  
458 X. Llopart, V. Gromov, R. Kluit, M. van Beuzekom, F. Zappone,  
459 V. Zivkovic, C. Brezina, K. Desch, Y. Fu, A. Kruth, Timepix3: a 65K  
460 channel hybrid pixel read out chip with simultaneous ToA/ToT and  
461 sparse read out, JINST 9 (05) (2014) C05013.  
462 URL <http://stacks.iop.org/1748-0221/9/i=05/a=C05013>
- 463 [7] J. Visser, M. van Beuzekom, H. Boterenbrood, B. van der Heijden, J. I.  
464 Muñoz, S. Kulis, B. Munneke, F. Schreuder, SPIDR: a read-out system  
465 for Medipix3 & Timepix3, Journal of Instrumentation 10 (12) (2015)  
466 C12028. doi:10.1088/1748-0221/10/12/C12028.
- 467 [8] B. van der Heijden, J. Visser, M. van Beuzekom, H. Boterenbrood,

- 468 S. Kulis, B. Munneke, F. Schreuder, SPIDR, a general-purpose read out  
469 system for pixel ASICs, JINST 12 (02) (2017) C02040. doi:10.1088/1748-  
470 0221/12/02/C02040.
- 471 [9] F. Hartjes, A diffraction limited nitrogen laser for detector calibration in  
472 high energy physics, Ph.D. thesis, University of Amsterdam (1990). URL  
473 [https://www.nikhef.nl/pub/services/biblio/theses\\_pdf/thesis\\_F\\_Hartjes.pdf](https://www.nikhef.nl/pub/services/biblio/theses_pdf/thesis_F_Hartjes.pdf)
- 474 [10] R. Diener et al., The DESY II test beam facility, Nuclear Instru-  
475 ments and Methods in Physics Research. Section A: Accelerators, Spec-  
476 trometers, Detectors and Associated Equipment 922 (2019) 265–286.  
477 arXiv:1807.09328, doi:10.1016/j.nima.2018.11.133.
- 478 [11] P. Baesso, D. Cussans, J. Goldstein, , Journal of Instrumentation 14 (09)  
479 (2019) P09019–P09019. arXiv:2005.00310.  
480 URL <https://doi.org/10.1088/1748-0221/14/09/p09019>
- 481 [12] D. Dannheim, K. Dort, L. Huth, D. Hynds, I. Kremastiotis, J. Kröger,  
482 M. Munker, F. Pitters, P. Schütze, S. Spannagel, T. Vanat, M. Williams,  
483 , Journal of Instrumentation 16 (03) (2021) P03008. doi:10.1088/1748-  
484 0221/16/03/p03008. arXiv:2011.12730.  
485 URL <https://doi.org/10.1088/1748-0221/16/03/p03008>
- 486 [13] R. Veenhof, Garfield - simulation of gaseous detectors, version 9, Refer-  
487 ence W5050 (1984-2010).  
488 URL <https://garfield.web.cern.ch>
- 489 [14] C. Kleinwort, General broken lines as advanced track fitting method,  
490 Nuclear Instruments and Methods in Physics Research Section A: Accel-

491 erators, Spectrometers, Detectors and Associated Equipment 673 (2012)  
492 107–110. doi:10.1016/j.nima.2012.01.024.

493 [15] S. F. Biagi, Monte Carlo simulation of electron drift and diffusion  
494 in counting gases under the influence of electric and magnetic fields,  
495 Nucl. Instrum. Meth. A421 (1-2) (1999) 234–240. doi:10.1016/S0168-  
496 9002(98)01233-9.

497 URL <https://magboltz.web.cern.ch/magboltz>